ACS APPLIED MATERIALS & INTERFACES
Research Article
Cite This: ACS Appl. Mater. Interfaces 2017, 9, 37094-37104
www.acsami.org

Visible-Blind UV Photodetector Based on Single-Walled Carbon Nanotube Thin Film/ZnO Vertical Heterostructures

Guanghui Li,[†,‡] Mohammad Suja,[§] Mingguang Chen,[†,‡] Elena Bekyarova,[†,‡,∥] Robert C. Haddon,[†,‡,∥,⊥] Jianlin Liu,[§] and Mikhail E. Itkis*[,†,‡,∥]

[†]Department of Chemical and Environmental Engineering, [‡]Center for Nanoscale Science and Engineering, [§]Department of Electrical and Computer Engineering, and [∥]Department of Chemistry, University of California, Riverside, California 92521, United States

Supporting Information

ABSTRACT: Ultraviolet (UV) photodetectors based on heterojunctions of conventional (Ge, Si, and GaAs) and wide bandgap semiconductors have been recently demonstrated, but achieving high UV sensitivity and visible-blind photodetection still remains a challenge. Here, we utilized a semitransparent film of p-type semiconducting single-walled carbon nanotubes (SC-SWNTs) with an energy gap of 0.68 ± 0.07 eV in combination with a molecular beam epitaxy grown n-ZnO layer to build a vertical p-SC-SWNT/n-ZnO heterojunction-based UV photodetector. The resulting device shows a current rectification ratio of 10^3, a current photoresponsivity up to 400 A/W in the UV spectral range from 370 to 230 nm, and a low dark current. The detector is practically visible-blind with the UV-to-visible photoresponsivity ratio of 10^5 due to extremely short photocarrier lifetimes in the one-dimensional SWNTs because of strong electron−phonon interactions leading to exciton formation. In this vertical configuration, UV radiation penetrates the top semitransparent SC-SWNT layer with low losses (10−20%) and excites photocarriers within the n-ZnO layer in close proximity to the p-SC-SWNT/n-ZnO interface, where electron−hole pairs are efficiently separated by a high built-in electric field associated with the heterojunction.

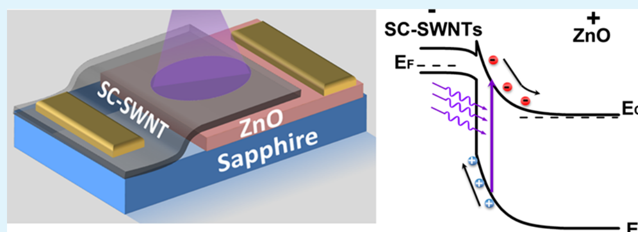

KEYWORDS: *carbon nanotubes, ZnO, UV photodetector, heterojunction, SWNT thin films*

1. INTRODUCTION

Single-walled carbon nanotubes (SWNTs) possess a unique combination of electrical and optical properties, originating from their one-dimensional (1D) structure, such as being metallic (MT) or semiconducting (SC) depending on their diameter and chirality.[1] Thin films of SWNTs can be prepared by a variety of techniques using scalable and manufacture-friendly solution-based processes, which are cost effective because of microgram quantities of SWNTs needed for large-area applications,[2−4] and with the choice of being made selectively of MT- or SC-SWNTs,[5] they provide a platform for development of a wide range of electronic and photonic applications, for example, large-area transparent conducting electrodes for touch screen displays, solar cells, light-emitting diodes (LEDs), and smart windows.[3,4,6−9] The bandgap of typical SC-SWNTs falls in the range of 0.6−1.2 eV, matching the bandgaps of conventional semiconductors such as Ge, Si, or GaAs. Patterning of SWNT thin films utilizing conventional lithography in combination with chemical and electrostatic doping of p- and n-types allowed to demonstrate all-SWNT thin film-based logical integrated circuits,[10,11] infrared photodetectors, and electrochromic devices with different functions performed by MT- and SC-SWNT counterparts.[12−17] The combination of SWNT thin films with conventional semiconductors resulted in the demonstration of high-performance vertical field-effect transistors and solar cells.[6,8]

ZnO is a wide bandgap semiconductor with a direct bandgap of 3.37 eV matching the spectral range desired for solid-state ultraviolet (UV) photodetectors for civil and military applications such as flame detection, UV-level monitoring for public health, intersatellite communication, early-warning missile detection, and engine flame control.[18−21] Schottky barrier types of ZnO photodetectors have some advantages over bulk ZnO photoconductors because of the built-in electric field efficiently separating the photoexcited electron−hole pairs before they recombine, and the performance of such devices has been improved by introducing an interdigitated electrode configuration.[21−26] p−n homojunction photodiodes are also utilized to generate a built-in electric field, but in the case of ZnO, this option is limited as a reliable growth technique for p-type ZnO is still under development.[20,27−30] The closest alternative to the ZnO p−n junction photodetector is a heterojunction device in which n-type ZnO is combined with a p-type conventional semiconductor, typically of a smaller bandgap, such as Si, Ge, or GaAs.[31−34] Such a heterojunction was shown to provide a high built-in electric field sufficient for the separation of photogenerated electrons and holes and a satisfactory photodetector performance, but an additional

Received: June 1, 2017
Accepted: September 26, 2017
Published: September 26, 2017

© 2017 American Chemical Society

DOI: 10.1021/acsami.7b07765
ACS Appl. Mater. Interfaces 2017, 9, 37094−37104

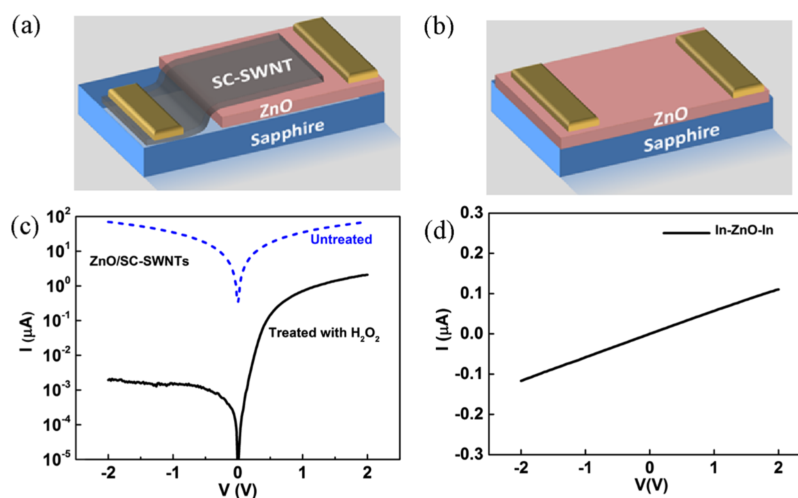

Figure 1. (a) Schematic of the vertical p-SC-SWNT/n-ZnO heterojunction; (b) structure of the lateral In−ZnO−In device; (c) *I*−*V* curves of the p-SC-SWNT/n-ZnO heterojunction before (dashed line) and after (solid line) hydrogen peroxide treatment; and (d) *I*−*V* curves of the lateral In−ZnO−In device.

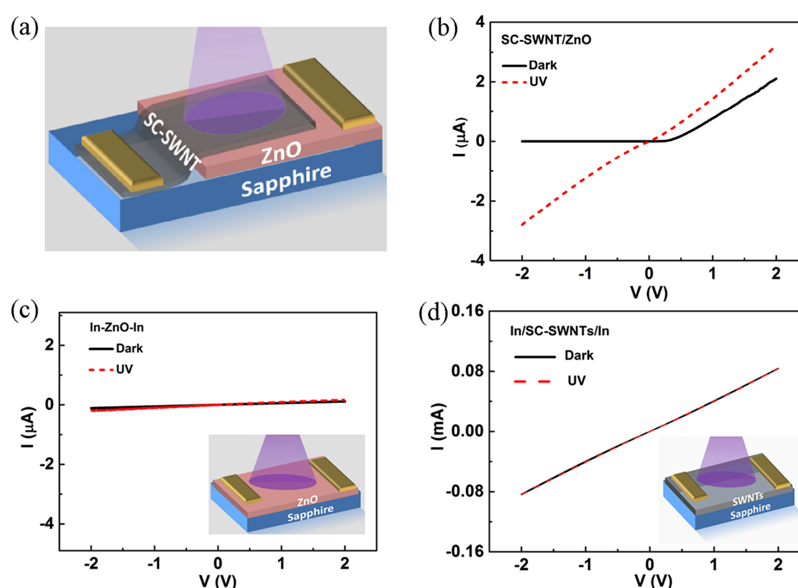

Figure 2. (a) Schematic of the p-SC-SWNTs/n-ZnO heterojunction under UV irradiation. *I*−*V* curves of the (b) SC-SWNT/ZnO heterojunction, (c) lateral In−ZnO−In device, and (d) lateral In−SWNT−In device in the dark (black solid curves) and under UV (370 nm, 3 $\mu W/cm^2$) irradiation (red dashed curves).

interface layer was needed to preclude unwanted visible spectral range sensitivity.[34] In addition to bulk ZnO layers, nanostructured forms of ZnO, such as nanoparticles and nanowires, have been explored,[35−45] showing improved performance in terms of higher UV responsivity,[37,38,41,43,45,46] and in some cases, faster response time.[37−42,44,46,47] Despite these recent advances, inorganic wide bandgap semiconductor-based UV photodetectors with visible blindness and fast response times still dominate the commercial market. Nevertheless, these photodetectors have a relatively low responsivity of ∼0.1 A/W. Thus, it is necessary to develop optimized device structures by the integration of a variety of new nanostructured materials for all-round competitiveness in the performance and manufacturability in the UV photodetector market.

In this paper, we used a highly transparent film of SC-SWNTs in place of a conventional semiconductor to build a vertical p-SC-SWNT/n-ZnO heterojunction, with a high current rectification ratio, capable of performing as a visible-blind UV photodetector with a high responsivity and low dark current. In this vertical configuration, UV radiation penetrates the top semitransparent SC-SWNT layer with low losses (10−20%) and excites the photocarriers within the n-ZnO layer in close proximity to the p-SWNT/n-ZnO interface where electron−hole pairs are efficiently separated by the high built-in electric field associated with the heterojunction.

2. RESULTS AND DISCUSSION

A schematic of the vertical p-SC-SWNT/n-ZnO heterojunction device is presented in Figure 1a. An n-type ZnO layer of 400 nm was grown on the *c*-sapphire substrate by the molecular beam epitaxy (MBE) technique (see Experimental Section for details).[28,48]

For this study, we utilized 99% SC-SWNTs of large diameter (1.5 ± 0.1 nm). We used the energy value of 0.68 eV

DOI: 10.1021/acsami.7b07765
ACS Appl. Mater. Interfaces 2017, 9, 37094−37104

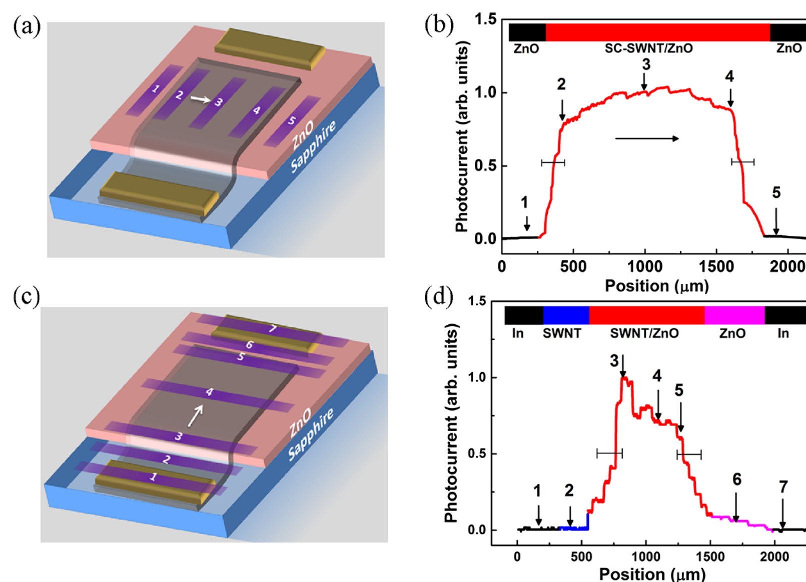

Figure 3. (a) Schematic of position-dependent photocurrent measurements across the width of the p-SC-SWNT/n-ZnO heterojunction device and (b) corresponding photocurrent measurements as a function of the position across the device at a reverse bias of −2 V. (c) Schematic of position-dependent photocurrent measurements along the length of the p-SC-SWNT/n-ZnO heterojunction device and (d) corresponding photocurrent measurements as a function of the position along the device at a reverse bias of −2 V. Horizontal error bars in (b,d) show a spatial resolution corresponding to the width of the slit diaphragm.

corresponding to the position of the maximum of the optical absorption in the lowest S_{11} absorption band (Figure S1) as the average bandgap for these SC-SWNTs. The width of the S_{11} absorption band at the half-maximum of absorption also gives the width of the bandgap distribution of ±0.07 eV for the ensemble of the SC-SWNTs. A rectangular fragment of the semitransparent SC-SWNT film with an effective thickness of 25 nm, length of 2 mm, and width of 1.2 mm was transferred on the ZnO layer. Prior to the SWNT film transfer, the ZnO layer was pretreated with hydrogen peroxide to tune the band bending and the conduction band offset at the p-SC-SWNT/n-ZnO interface.[21,49−51] Two indium electrodes were deposited to complete the device fabrication: one electrode provides electrical contact to the top SC-SWNT film layer (just outside the ZnO layer), and the second electrode addresses the bottom ZnO layer just outside the SC-SWNT film. This configuration carries some lateral motif as the charge carriers travel in a lateral direction along the SWNT thin film and ZnO layer before entering or exiting the vertical heterojunction. However, as we show below, the voltage drop associated with such a lateral current is several orders of magnitude smaller than the voltage drop across the heterojunction when it is reverse-biased, hence, it effectively acts as a vertical heterojunction. For comparison, a lateral n-ZnO device of the same area with two indium electrodes, as shown in Figure 1b, was investigated.

Figure 1c shows the *I*−*V* characteristics of p-SC-SWNT/n-ZnO heterojunction devices with and without hydrogen peroxide pretreatment of the ZnO surface. Without the pretreatment, no significant rectification was observed, whereas the device with the pretreated ZnO surface showed a significant degree of rectification of about 10^3 at ±2.0 V. By contrast, the lateral ZnO device with the pretreated ZnO surface layer shows a linear *I*−*V* curve (Figure 1d) corresponding to ohmic In−ZnO contacts and a lateral resistance of the ZnO layer of 7×10^5 Ω. Additional measurements provide a value of lateral resistance of the SC-SWNT film of ∼20 kΩ, as shown below. It should be noted that in any vertical optoelectronic device, the lateral travel of the carriers is inevitable, independent of the nature of the top transparent conducting electrode, but the resistance and voltage drop associated with such a lateral current should be minimized. Both lateral resistances are orders of magnitude smaller than the total resistance of the device of 10^9 Ω at a negative bias of −2.0 V, which is dominated by the resistance of the heterojunction, thus supporting the earlier statement of functionally dominating vertical motif of the device architecture.

Figure 2a presents the sketch of the heterojunction device under UV illumination, and Figure 2b shows the *I*−*V* curves of the p-SC-SWNT/n-ZnO heterojunction device in the dark and under illumination from an ultraviolet LED (central wavelength λ = 370 nm) of an incident light intensity of 3 μW/cm^2 (power P = 75 nW).

Multiple p-SC-SWNT/n-ZnO heterojunction devices were prepared following the procedure described above, showing a similar dark rectification of the *I*−*V* curve and a similar photoresponse to UV irradiation (Figure S2). At a negative bias of −2.0 V, the dark current is 2 nA and the photocurrent approaches 3 μA, which corresponds to a UV photoresponsivity of 40 A/W. In comparison, the lateral In−ZnO−In device shows a much lower photoresponsivity of <1 A/W and a much higher dark current of 120 nA, as shown in Figure 2c. As an alternative to the vertical architecture, the lateral device can be improved by introducing a Schottky barrier-type interdigitated electrode configuration with a higher width-to-length aspect ratio and a higher photocarrier collection efficiency associated with a shorter interelectrode distance, with the presence of the Schottky barrier introducing a high built-in electric field separating the photoexcited electron−hole pairs at the ZnO−metal interface.[24−26] Figure 2d shows the *I*−*V* characteristics of a p-SC-SWNT film of the same thickness and lateral dimensions as the heterojunction device with similar indium electrodes. These *I*−*V* curves are linear, with the slope corresponding to the value of the lateral resistance of the SC-SWNT film of ∼20 kΩ, and no measurable photocurrent was

DOI: 10.1021/acsami.7b07765
ACS Appl. Mater. Interfaces 2017, 9, 37094−37104

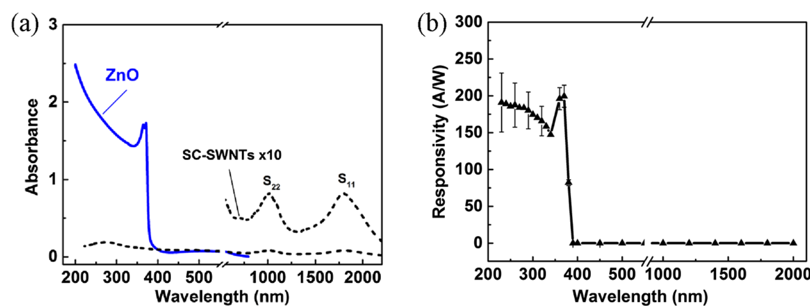

Figure 4. (a) UV−vis−NIR absorption spectra of ZnO (blue solid curve) and SC-SWNT thin films (black dashed curve); (b) spectral dependence of the photoresponsivity of the SC-SWNT/ZnO heterojunction at the incident power of 10 nW (light intensity of 250 nW/cm^2) at −2 V bias.

observed under UV illumination. We should note that the indium electrode would make a Schottky-type contact to the p-type individual SWNT, and the corresponding $I-V$ curve would have been nonlinear. However, in the case of the macroscopic (mm size) SWNT thin film, the total resistance of the SWNT network is usually dominated by the resistances of thousands of intertube junctions with negligible contact resistance between the large-area indium electrode and the SWNT film (as confirmed by 4-probe measurements), resulting in the linear $I-V$ curve as shown in Figure 2d.

The presented comparison of the performance of individual components of the device indicates that the introduction of a vertical structure with the p-SC-SWNT/n-ZnO heterojunction provides a significant gain of UV photoresponse in comparison with utilization of the same n-ZnO UV-sensitive layer in a lateral configuration. To verify this point, a micrometer-controlled narrow slit diaphragm of width 200 μm was used to measure the device photoresponse as a function of the position of the illumination spot across the width of the device, as schematically shown in Figure 3a. The scan width includes the areas of the ZnO layer not coated with the SC-SWNT film (see positions 1 and 5 in Figure 3a). The resulted photoresponse scan is presented in Figure 3b and shows high photocurrent values of ∼1 μA when the UV light (λ = 370 nm) illuminates the area of the p-SC-SWNT/n-ZnO heterojunction (positions 2−4) and a decrease of photocurrent by 50−100 times when the UV-irradiated spot moves from the SC-SWNT film to the adjacent ZnO area (positions 1 and 5).

Another scan was conducted along the length of the device across the space between indium electrodes, as illustrated in Figure 3c, and the results of the scan are presented in Figure 3d. To conduct this scan, the heterojunction device was modified by increasing the length of the uncovered ZnO layer between the edge of the SC-SWNT film and the indium electrode from 100 to 500 μm, whereas the length of the heterojunction area in this device was 700 μm. The scan showed no photoresponse in the SC-SWNT film area adjacent to the first indium electrode (position 2), showed a strong photoresponse in the central area where the ZnO and SWNT layers overlap (positions 3−5), and a significant drop in the photoresponse in the area adjacent to the second indium electrode where only the ZnO layer is present. Thus, to achieve an efficient UV photoresponse, the photoexcited carriers should be generated in the ZnO layer covered by the SWNT film in the vicinity of the p-SC-SWNT/n-ZnO interface.

UV−vis−NIR (ultraviolet−visible−near-infrared) absorption spectra of the ZnO and SC-SWNT layers and the spectral dependence of the photoresponse are presented in Figure 4a,b, respectively. The onset of strong absorption in the ZnO layer appears at a wavelength near 380 nm with the absorption maximum (ABS = 1.8) at 370 nm in agreement with the known bandgap of ZnO of 3.37 eV.[18−20] Absorption of the semitransparent 25 nm thick film of SC-SWNT is only 0.1 at 370 nm (transmittance of 79%) because of its small thickness that is sufficient to form the heterojunction and at the same time to function as a transparent conducting electrode. The UV absorption averages 0.15 in the range of SWNT π-plasmon maximum of 220−330 nm. The thickness of the SWNT film can be further decreased to less than 10 nm (transmittance >90%) to reduce the loss of UV light intensity. The characteristic absorption bands S_{11} and S_{22} corresponding to the set of separations between van Hove singularities of 1D SC-SWNTs appear in the NIR spectral range centered around wavelengths 1750 and 1000 nm, respectively, with the maximum of absorption not exceeding a value of 0.1 in the NIR and visible spectral ranges, as shown in Figures 4a and S1b.

Figure 4b shows the spectral responsivity of the p-SC-SWNT/n-ZnO heterojunction device. The onset of photoconductivity appears at 380 nm with the photoresponsivity reaching ∼200 A/W at 370 nm and extending from UV-A to UV-B and UV-C spectral range at least up to a wavelength of 230 nm, the spectral limit of our instrumentation. These photoresponsivity values are on the high end of the typical values achieved for UV photodetectors,[18−20,36−41] however recently, much higher photoresponsivity values such as 26 000 and 1.7 × 10^6 A/W were reported for interdigitated Au/ZnO and ZnO quantum dot/carbon nanodot-based devices, respectively.[43,45]

In the visible spectral range, the photoresponse drops practically to zero; more accurate responsivity measurements utilizing blue (λ = 470 nm), yellow (λ = 520 nm), and red (λ = 630 nm) LEDs with the incident power in the range of 1 μW to 0.2 mW were performed. For blue and red LEDs, a measurable photoresponse was observed, and the resulting responsivities were evaluated at the level of 10^{-3} and 1 × 10^{-5} A/W, respectively (Figure S3). For the yellow LED, no measurable photoresponse was observed as the power was limited to 5 μW, and the level of responsivity not exceeding 4 × 10^{-5} A/W was estimated from the measured noise of the photodetector current under a reverse bias of −2 V. Thus, we conclude that the current responsivity in the visible range does not exceed 0.001 A/W, and the UV-to-visible light responsivity ratio exceeds 10^5, making the p-SC-SWNT/n-ZnO heterojunction photodetector, practically visible-blind. The visible blindness is an important benefit for the UV photodetector application, taking into account the high intensity of the background visible radiation in the typical UV photodetector applications.

DOI: 10.1021/acsami.7b07765
ACS Appl. Mater. Interfaces 2017, 9, 37094−37104

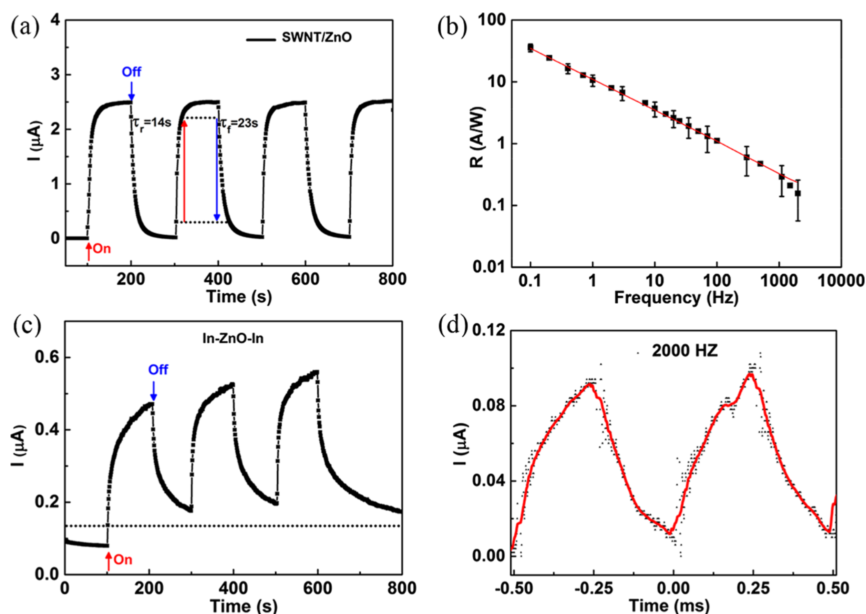

Figure 5. (a) Temporal photoresponse of the p-SC-SWNT/n-ZnO heterojunction device under 370 nm light at a frequency of 0.005 Hz; (b) frequency dependence of photoresponse under an UV light intensity of 2 μW/cm^2 (squares); straight lines correspond to the $R \propto f^{-\alpha}$ fitting with α = 0.5; (c) temporal photoresponse of the In−ZnO−In lateral device under 370 nm light at a frequency of 0.005 Hz (V_{bias} = −2 V); (d) oscilloscope traces of photoresponse of the p-SC-SWNT/n-ZnO heterojunction device at 2000 Hz. V_{bias} = −2 V for all plots (a−d).

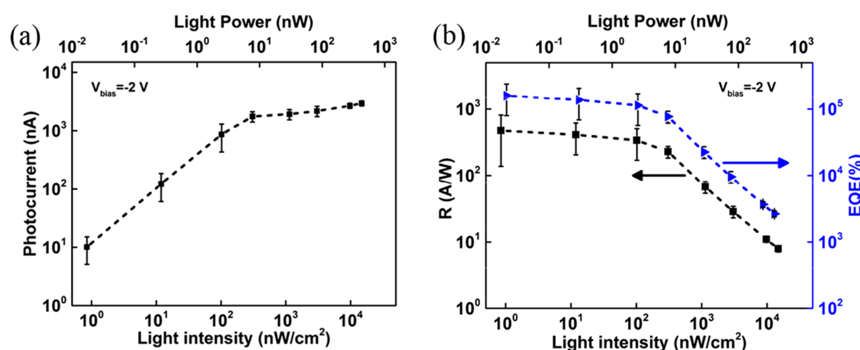

Figure 6. (a) Photocurrent and (b) photoresponsivity (black squares) and external quantum efficiency (EQE, blue triangles) of the p-SC-SWNT/n-ZnO heterojunction device as a function of the incident 370 nm light intensity at a reverse bias of −2 V.

It should be noted that graphene is an alternative carbon-based nanostructured material, which has been utilized as a transparent conducting electrode for a wide range of optoelectronic applications, and it can also be n- or p-doped depending on the application needs.[52] Recently, several reports presented UV photodetectors based on junctions of graphene with arrays of ZnO nanowires or nanorods, demonstrating high UV range responsivity up to 113 A/W and millisecond range response times.[38,53] However, these graphene-based photodetectors are not visible-blind as they show photosensitivity not only in the UV range but also in the visible and NIR ranges, which was associated with either continuous spectral absorption in the gapless graphene or defects in the ZnO and graphene layers.[38,53]

Figure 5a presents the temporal photoresponse of the p-SC-SWNT/n-ZnO heterojunction device to square-wave pulses of UV radiation of an incident power of 3 μW/cm^2 generated by UV LED (λ = 370 nm) electrically modulated at a low frequency of 0.005 Hz. It shows a relatively fast onset of the photocurrent followed by a slow approach to saturation with 10−90% rise and decay times of 14 and 23 s, respectively. Frequency dependence of the photoresponse is presented in Figure 5b: it shows decreasing responsivity R with increasing frequency, which can be fitted to $R \propto f^{-\alpha}$ dependence, with exponent α = 0.5 usually associated with a wide distribution of lifetimes of the photoexcited carriers in the range of tens of seconds to milliseconds. For comparison, the temporal response of the lateral In−ZnO−In device measured under the same irradiation conditions is presented in Figure 5c. It shows significant non-zero dark current and ∼6 times smaller amplitude of the current modulation. Corresponding 10−90% rise and decay times exceed 100 and 600 s, respectively. Thus, introduction of the SWNT/ZnO heterojunction not only enhances the amplitude of the photoresponse but also makes it significantly faster in comparison with the lateral In−ZnO−In device. In fact, a measurable photoresponse of the SWNT/ZnO heterojunction device can be observed up to a frequency of 2000 Hz, as can be seen in the oscilloscope traces presented in Figure 5d.

Figure 6a presents dependences of the photocurrent on the incident power of the UV radiation at the LED central wavelength λ = 370 nm. At the UV light intensity range of 1−

DOI: 10.1021/acsami.7b07765
ACS Appl. Mater. Interfaces 2017, 9, 37094−37104

100 nW/cm^2, a practically linear relationship between the photocurrent and incident power is observed, which changes to a sublinear dependence with a tendency to saturation on further increase in the incident power. Figure 6b presents the corresponding photoresponsivity R. At a lower incident UV light intensity below 100 nW/cm^2, the responsivity reaches 400 A/W, which is on the high end of the typical values reported for UV detectors,[18−20,36−41] although much higher values up to 1.7 × 10^6 A/W have been reported recently.[43,45]

With increasing light intensity above 400 nW/cm^2, the photoresponsivity decreases below 100 A/W, but sustains quite a high value of ∼10 A/W at an incident power of a few μW/cm^2. Such a tendency of the photoresponse toward saturation and the corresponding photoresponsivity decrease with increasing power indicate an involvement of the trap states in the mechanism of photoconductivity, as we discuss below.

The EQE of the photodetector can be evaluated at the wavelength λ = 370 nm using the following equation

$$\text{EQE}\ \% = \frac{R \times 1240}{\lambda} \times 100 \quad (1)$$

The resulting plot of EQE as a function of the UV light intensity is presented in Figure 6b and shows a high EQE value up to 1.0 × 10^5%, indicating a high photocurrent gain associated with long photocarrier lifetimes because of the efficient separation of photoexcited electrons and holes.

A major figure of merit of the UV photodetector performance specific detectivity, D^*, is often evaluated on the basis of quasi-static measurements using the following equation under the assumption that the noise current is dominated by the shot noise from the dark current I_{dark} of the device[37,40,41,54]

$$D^* = \frac{R}{(2e \times I_{\text{dark}}/A)^{1/2}} \quad (2)$$

where R is the current responsivity (A/W), e is the electron charge (1.6 × 10^{-19} C), and A is the effective area of the photodetector. Using the experimental dark current value of 2 nA at a reverse bias of −2 V and an active detector area of 2 × 1.2 mm^2 (0.024 cm^2), D^* = 3.2 × 10^{15} Hz$^{1/2}$·cm/W can be obtained, which is comparable to the best values reported for UV photodetectors under the same noise origin assumptions.[37,39,40] A more general evaluation of the detectivity D^* can be obtained on the basis of the following equation[55]

$$D^* = \frac{(A\Delta f)^{1/2}}{\text{NEP}} = \frac{R(A\Delta f)^{1/2}}{I_n} \quad (3)$$

where NEP is the noise equivalent power of the detector at the UV light modulation frequency f, I_n is the root-mean-square value of the measured noise current in the detector circuit in the electrical bandwidth Δf (Hz), and the relationship NEP = I_n/R is utilized. For calculations at the UV light modulation frequency of 10 Hz, experimental values of the current responsivity and noise current of 30 A/W and 6 × 10^{-12} A, respectively, were utilized resulting in NEP = 2 × 10^{-13} W/Hz$^{1/2}$ and a more realistic value of D^* = 0.8 × 10^{12} (Hz$^{1/2}$·cm)/W. Such a difference in D^* values obtained using eqs 2 and 3 indicate that in addition to shot noise, other sources of noise such as "flicker" (1/f) noise and Johnson noise are important in the case of our p-SC-SWNT/n-ZnO heterojunction, and further optimization of the components of the heterojunction device is required. For example, decreasing the series resistance of the photodetector by optimizing the preparation and processing of the ZnO layer can significantly reduce both Johnson and 1/f noises and improve the linearity of the detector response.

Majority of studies on ZnO-based UV photodetectors and other inorganic UV detectors report responsivity values in the range of 1 mA/W to 10 A/W and response times of a few seconds to hundreds of seconds, typically limited by oxygen desorption−absorption processes under UV irradiation.[18,19,36,37,56] Faster response times in the subsecond range were recently reported on ZnO-based nanostructured systems, but with responsivities in the mA/W range.[57] High responsivity values in the range of 100−1000 A/W were reported for nanostructured forms of ZnO,[38,41,46] and, recently, a significant enhancement of the responsivity up to 1.7 × 10^6 A/W was reported.[43,45] Also, in some of the recent reports the response time was reduced to milliseconds and in the sub-millisecond range, however, with a reduced UV-to-visible responsivities ratio (<100).[38,41] In our p-SC-SWNT/n-ZnO heterojunction UV detector, a significant response can be observed up to a frequency of 2000 Hz (Figure 5d), indicating the presence of fast processes, which can be potentially enhanced by tuning the properties of SWNT and ZnO layers, their geometry, and the photocarrier extraction pathways.

To describe the current transport in our p-SC-SWNT/n-ZnO heterojunction device in the dark and under UV illumination, we applied a model developed for the case of the p-Ge/n-GaAs heterojunction.[58,59] It should be noted that the SC-SWNT film itself presents a complex network of entangled SWNTs with the electrical transport limited by the charge carriers hopping (tunneling) across the intertube junctions, whereas here, for simplicity, the SC-SWNT layer is treated as a bulk conventional semiconductor with bandgap E_g ≈ 0.68 eV,[60] evaluated from the absorption spectrum of the SC-SWNT film (Figure S1) and close to E_g of Ge of 0.67 eV at 300 K.[60] The band diagram schematic of p-SC-SWNT and n-ZnO layers after establishing the heterojunction is presented in Figures 7a and S4 in more detail.

For construction of the band diagram, the work function and electron affinity χ_{SWNT} of p-type SC-SWNTs are 4.3 and 4.8 eV, respectively, based on the literature report.[8,61,62] The electron affinity of ZnO, χ_{ZnO}, is 4.0 ± 0.2 eV.[18−21,63] According to Anderson consideration of the heterojunction, the conduction band discontinuity ΔE_c is equal to the difference in the electron affinities of the contacting materials, thus giving $\Delta E_c = \chi_{\text{SWNT}} - \chi_{\text{ZnO}} \approx 0.3 \pm 0.1$ eV,[58,59] and the corresponding valence band discontinuity ΔE_v can be estimated as $\Delta E_v = E_{\text{gZnO}} - E_{\text{gSWNT}} - \Delta E_c \approx 2.4$ eV.[58,59] With the majority carrier (electron) concentration in n-ZnO of n ≈ 2.9 × 10^{17} cm^{-3} obtained from Hall effect measurements, the minority carrier (hole) concentration p is extremely low (p ≈ 1.7 × 10^{-37} cm^{-3}), and the calculated Fermi level position is 0.07 eV below the conduction band edge E_c, as described in detail in the Supporting Information. The hole and electron concentrations in environmentally p-doped SC-SWNTs were estimated at the level of p_{SWNT} ≈ 5 × 10^{19} and n_{SWNT} ≈ 6 × 10^{13} cm^{-3}, respectively, as discussed in the Supporting Information. The corresponding hole and electron linear concentrations (per p-SC-SWNT length) are estimated as ∼1.4 × 10^5 and ∼1.7 × 10^{-1} cm^{-1}, respectively.

According to previous reports, hydrogen peroxide treatment leads to the removal of highly conducting electron accumulation layer formed by several monolayers of hydroxide and generation of Zn vacancies within a depth of few hundred

DOI: 10.1021/acsami.7b07765
ACS Appl. Mater. Interfaces 2017, 9, 37094−37104

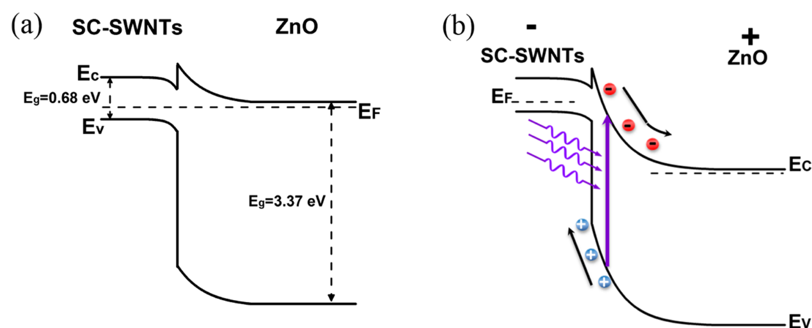

Figure 7. (a) Band diagram of the p-SC-SWNT/n-ZnO heterojunction under zero bias; (b) band diagram of the p-SC-SWNT/n-ZnO heterojunction under reverse bias and UV illumination, showing photoexcitation of electron−hole pairs and their separation in the ZnO layer in the vicinity of the heterojunction interface.

nanometers, resulting in upward band bending in the vicinity of the p-SC-SWNT/n-ZnO interface up to 0.6 eV, which correlates with our experimental observation of 4-fold increase in the lateral resistance of the ZnO layer.[50,63] In addition, during the heterojunction formation, the work function difference forces the electron transfer from n-ZnO to p-SC-SWNTs, resulting in an increase of upward band bending in the n-ZnO layer close to the interface and the corresponding downward band bending in the p-SC-SWNT layer. The downward band bending at the SC-SWNT side toward the intrinsic state is confirmed by the observed ∼3 times increase in the lateral resistance of the SC-SWNT layer compared to a similar SC-SWNT film transferred to a glass substrate. It also correlates with the partial restoration of the strength of the S_{11} absorption band after transfer of the SWNT film on the top of the ZnO layer, as would be expected in the case of reduced average level of p-doping across the thickness of the SC-SWNT layer. The distance between the Fermi level and the peak value of E_c in ZnO estimated to be $\phi_b = 0.64 \pm 0.1$ eV (see the Supporting Information), which together with the conduction band discontinuity ΔE_c of $\sim 0.3 \pm 0.1$ eV, is responsible for the high rectification ratio of the $I-V$ curve. Fitting of the experimental $I-V$ curve to the expression describing the thermionic emission across the Schottky barrier at the metal−semiconductor junction (Figure S5)[64] gave a value of series resistance $R_S = 700$ kΩ and a Schottky barrier height of 0.806 eV. This number is larger than the above value of $\phi_b = 0.64 \pm 0.1$ eV, which may be due to the limitations of the utilized Schottky barrier approximation.

Under the reverse bias (negative polarity on the SWNT side), the flow of holes (minority carriers in n-ZnO) to the SC-SWNT layer can be neglected because of the large bandgap and n-type doping of the ZnO layer, and the overall current is provided by electron transport from SWNTs to ZnO. The $I-V$ curve in Figure 1c shows that the reverse current remains low at the level of ∼2 nA as it is limited by the barrier ϕ_b, which also includes the conduction band discontinuity ΔE_c. The forward dark current is ∼3 orders of magnitude larger than the reverse current at a similar bias because of the reduced band bending at the n-ZnO side and is dominated by the electron (n-ZnO majority carriers) flow into the SC-SWNT layer as the hole component of the current from SWNTs to ZnO should be negligible because of a large barrier ΔE_v corresponding to the valence band discontinuity. This description does not take into account the tunneling and recombination processes, which may be important for the current transport across the heterojunction.[65]

The mechanism of photocurrent of the p-SC-SWNT/n-ZnO heterojunction is illustrated qualitatively in Figure 7b. UV illumination with photon energies higher than the bandgap of ZnO of 3.37 eV ($\lambda < 368$ nm) enters ZnO after passing through the semitransparent SC-SWNT layer with small losses (∼10−20%) and excites electron−hole pairs in close proximity to the SC-SWNT/n-ZnO heterojunction interface in the region of the maximum band bending and the highest built-in electric field. The reverse bias further enhances the band bending and the electric field on the ZnO side in the vicinity of the p-SC-SWNT/n-ZnO interface, leading to efficient separation of photoexcited electrons and holes before they recombine. The photoexcited holes are being swept into the SC-SWNT layer and electrons from the depleted high resistance ZnO interface layer to the bulk (deep) n-ZnO layer of higher electrical conductivity. In this configuration, the p-doped SC-SWNT film acts as a transparent electrode and also as a hole current collector simultaneously, whereas the deep n-ZnO layer acts as an electron current collector delivering photoexcited electrons and holes toward the respective indium ohmic contacts, thus completing the photocurrent circuit.

The improved photoresponse is associated with the most efficient use of the whole area of the heterojunction, which is illuminated by UV light through the highly transparent SC-SWNT film and the preferential photoexcitation of electron−hole pairs in the region of the highest built-in electric field, leading to the efficient separation and collection of photoexcited carriers. Relatively large barrier $\phi_b = 0.64 \pm 0.1$ eV, which also includes the conduction band discontinuity $\Delta E_c \approx 0.3$ eV limits the dark current to the low value of ∼2 nA resulting in a high on/off contrast. The frequency dependence of photoresponsivity $R \propto f^{-\alpha}$ with exponent $\alpha = 0.5$ (Figure 5b) indicates a wide distribution of lifetimes of photoexcited carriers and points out to the contribution of traps, such as Zn vacancies, capturing and releasing one type of carriers, thus extending the photocarrier lifetimes and enhancing the photocurrent but also slowing down the photoresponse.[66] At a high intensity of UV radiation, the limited concentration of the available trap states and a shift of the quasi-Fermi level in ZnO lead to a saturation of the photoresponse, as observed in Figure 6a.[66] Another possible cause of saturation is the relatively high series resistance of the ZnO layer limiting the photocurrent.

The photons with energy below the ZnO bandgap but higher than the bandgap of SC-SWNTs ($E_g = 0.68$ eV) are capable of exciting the electron−hole pairs within the SC-SWNT layer, but the strong electron−phonon interaction in 1D-SWNTs

DOI: 10.1021/acsami.7b07765
ACS Appl. Mater. Interfaces 2017, 9, 37094−37104

leads to the formation of exciton-bound states within the time frame of less than 10^{-12} s, followed by the energy relaxation to the lattice phonons, (heat) as shown by the theoretical study[67] and experimentally utilizing time-resolved fluorescence,[68] polarized pump−probe photomodulation and photoluminescence,[69] two-photon excitation technique,[70] and bolometric spectroscopy.[12] This difference in UV and visible mechanisms of photoexcitation in ZnO and SC-SWNTs, respectively, leads to the observed high UV-to-visible photoresponsivity ratio exceeding 10^5.

Under a forward bias, a positive photocurrent was observed leading to a quasi-linear *I*−*V* curve under UV light irradiation, which is unusual for the case of a photodiode or heterojunction-based photodetectors. It should be noted that the equivalent circuit of the heterojunction (or photodiode) includes a series resistor of the ZnO layer, which is quite large (700 kΩ) in our heterojunction device and originates from the lateral flow of the charge carriers in the ZnO layer. Thus, some contribution to the positive photoresponse in the forward bias can come from the ZnO layer acting as a photoresistor. On the other hand, similar observations of positive photoresponse in the forward bias and a linear *I*−*V* curve were reported for the cases of Au−ZnO nanowire−Au device and graphene−ZnO nanorod device.[38,71] In those reports, it was suggested that the holes generated by UV irradiation refill (compensate) the deep traps responsible for the depletion region and the upward band bending in the ZnO layer adjacent to the interface, thus reducing the height of the potential barrier responsible for the rectification of the *I*−*V* curves, which can be an alternative explanation for the nature of the photoresponse observed in our SWNT/ZnO heterojunction device. The exact nature of the photoresponse needs to be clarified in future studies.

The detector performance can be further optimized by tuning the degree of doping of the SWNT and ZnO layers, the thickness of both layers, and the surface treatment of ZnO for further improvement of the rectification ratio and enhancement of internal electric field for more efficient separation and extraction of photoexcited carriers. The linearity (dynamic range) of the response can be improved by decreasing the series resistance of the device associated with the lateral transport of extracted photocarriers along the ZnO layer. An alternative to SC-SWNT/ZnO can be the MT-SWNT/ZnO junction, which would correspond to vertical Schottky barrier rather than the heterojunction type of a photodetector. For practical applications, a fast response time is extremely important; hence, the nature of the interface and bulk states controlling the photocarrier lifetimes needs to be elucidated and optimized by varying the ZnO layer growth technique and conditions, its surface processing, and the SWNT layer transfer during the formation of the heterojunction with an ultimate target to decrease the response time from 10 s to millisecond range.

3. CONCLUSIONS

UV photodetector was built on the basis of a semitransparent p-SC-SWNT thin film/n-ZnO vertical heterojunction. The device constitutes a simple planar two-layer structure: after the initial MBE growth of the ZnO layer, the device preparation can be completed by the solution-based SWNT thin film preparation and transfer; hence, both large- and small-area devices can be prepared by this technique, and the patterning can be added to prepare an array or modify the geometry of such photodetectors. The novelty and merit of the introduced SC-SWNT/ZnO vertical heterojunction device is in the efficiency of the SC-SWNT layer to enhance the UV performance of ZnO, as shown by the comparison with the lateral ZnO device made on the basis of the identical ZnO layer. In this vertical device architecture, the SC-SWNT thin film serves two functions simultaneously, namely, as a transparent conducting electrode and as a semiconducting material forming the heterojunctions. Thus, the multifunctionality of the SWNT thin films is fully utilized. The resulting UV photodetector shows a high responsivity up to 400 A/W at a wavelength range of 370−230 nm and is visible-blind with the UV-to-visible photoresponsivity contrast ratio exceeding 10^5. The detector operates at a relatively low reverse bias of 1−2 V and shows dark current rectification ratio of 10^3. The p-SC-SWNT/n-ZnO heterojunction is rationalized in terms of the model developed for the heterojunction of conventional bulk semiconductors, such as p-Ge/n-GaAs.[58,59,64] The mechanism of photodetection includes efficient separation of photoexcited electron−hole pairs in the strong built-in electric field on the ZnO side of the heterojunction, with the involvement of the interface and bulk ZnO intragap states trapping and releasing photoexcited carriers, thus increasing the photocarrier lifetimes. The presented approach illustrates a synergistic improvement of the UV detector performance when carbon nanomaterials and wide bandgap semiconductors are combined in a single device architecture.

4. EXPERIMENTAL SECTION

4.1. Preparation of the ZnO Layer. The ZnO thin film was grown on the *c*-sapphire (0001) substrate by a radio frequency (rf) plasma-assisted SVTA (SVT Associates, Inc.) MBE system. High-purity elemental Zn (6 N) and Mg (6 N) were evaporated using Knudsen effusion cells, and high-purity O_2 (6 N) gas flow controlled by a mass flow controller was directed to the RF plasma source to generate active oxygen radicals. The sapphire substrate was cleaned in aqua regia (HCl/HNO_3) solution at a temperature of 150 °C for 40 min, rinsed in deionized (DI) water, blown dry by nitrogen gas, and transferred immediately to the MBE chamber. The substrate was then annealed in vacuum at 800 °C for 15 min to achieve an atomically clean surface. The growth procedure followed several steps. At first, a MgO/ZnO (∼3 nm/8 nm) low temperature buffer layer was deposited on the substrate at a substrate temperature of 450 °C for 5 min. During the buffer layer growth, the effusion cell temperature for Mg and Zn was maintained at 450 and 320 °C, respectively, whereas the O_2 flow rate was 2 sccm. The buffer layer minimizes the lattice mismatch between ZnO and the *c*-sapphire substrate. In the next step, the ZnO layer was deposited at a substrate temperature of 600 °C, a Zn cell temperature of 340 °C, and an O_2 flow rate of 2.5 sccm for a growth duration of 3 h. In the final step, the ZnO film was annealed in situ at 700 °C for 20 min with an O_2 flow rate of 1.5 sccm. The RF plasma power of 400 W was maintained throughout the whole growth period. The ZnO film yields a total thickness of ∼400 nm. Although the film was not intentionally doped, it exhibits n-type behavior with a carrier density of 2.9×10^{17} cm^{-3} and a resistivity of 6.2 Ω·cm.

4.2. Device Fabrication. The ZnO film grown on the sapphire substrate was treated by 30% H_2O_2 solution (Fisher Chemical) for 3 min at 100 °C, washed in DI water, and dried under nitrogen gas flow according to the procedure described in the literature.[50,51] The aqueous dispersion of 99% SC-SWNTs of large diameter (∼1.5 ± 0.1 nm) was purchased from NanoIntegris Inc. Semitransparent SC-SWNT thin films were prepared by vacuum filtration of the SC-SWNT dispersion utilizing the cellulose membrane (Millipore, type VMWP, pore size 0.05 μm) and transferred on the ZnO layer via the membrane dissolution in acetone vapor and additional washing in acetone and DI water. The thickness of the SC-SWNT film was defined by the amount of filtered SC-SWNT material, taking into account the effective area of the membrane and assuming a SWNT film density of 1 g·cm^{-3}, as described in our previous reports.[16,17] The

DOI: 10.1021/acsami.7b07765
ACS Appl. Mater. Interfaces 2017, 9, 37094−37104

thickness was confirmed by measurement of the optical density of the SC-SWNT layer.[72]

4.3. Electrical and Photoelectrical Device Characterization. Current−voltage ($I-V$) measurements were conducted utilizing a Keithley 236 source-measure unit employing LabView-based acquisition system. UV−vis−NIR spectra of ZnO and SC-SWNT films and photoconductivity spectra were collected using a Cary 5000 spectrophotometer (Agilent Technologies). Calibrated wide bandgap semiconductor GaP UV photodetector (GaP, model FGAP71, Thorlabs) was used to measure the incident UV light intensity. LED (model 370E, Thorlabs) with a central wavelength of 370 nm was used as the source of UV radiation for the single wavelength measurements. The LED irradiation was modulated using a function generator SRS-DS345 (Stanford Research Systems), and the amplitude of the photoresponse under various light intensities and modulation frequencies were studied using a lock-in amplifier (SRS 830, Stanford Research Systems). The noise voltage V_n on the load resistance R_L = 10 kΩ (Δf = 1 Hz bandwidth) at different frequencies f of UV light modulation was measured using the SRS 830 lock-in amplifier signal-processing capabilities and converted to the noise current $I_n = V_n/R_L$, where R_L is the load resistance in the detector bias circuit. The temporal traces of the photoresponse were collected using a Tektronix TDS 1001C-EDU oscilloscope.

■ ASSOCIATED CONTENT

Supporting Information

The Supporting Information is available free of charge on the ACS Publications website at DOI: 10.1021/acsami.7b07765.

Absorption spectrum of the film of SC-SWNTs, $I-V$ curves of several SWNT/ZnO devices in the dark and under UV illumination, comparison of photoresponsivities in UV and visible spectral ranges, schematic and detailed discussion of the band diagram of the vertical SWNT/ZnO heterojunction, calculation of the Fermi level in ZnO, and fitting of the $I-V$ curve (PDF)

■ AUTHOR INFORMATION

Corresponding Author

*E-mail: mitkis@engr.ucr.edu.

ORCID

Mingguang Chen: 0000-0002-8261-3657

Mikhail E. Itkis: 0000-0003-2447-2267

Notes

The authors declare no competing financial interest.

[⊥]R.C.H.—deceased on April 21, 2016.

■ ACKNOWLEDGMENTS

We gratefully acknowledge the financial support of the National Science Foundation under contract ECCS-1404671 and the support provided by the Vice Chancellor for Research and Economic Development, University of California, Riverside. The ZnO growth for device fabrication was also supported by SHINES, an Energy Frontier Research Center funded by the US Department of Energy, Office of Science, Basic Energy Sciences under Award #SC0012670.

■ REFERENCES

(1) Dresselhaus, M. S.; Dresselhaus, G.; Avouris, P. *Carbon Nanotubes: Synthesis, Structure, Properties and Applications*; Springer-Verlag: Berlin, 2001; Vol. *80*.

(2) Wu, Z.; Chen, Z.; Du, X.; Logan, J. M.; Sippel, J.; Nikolou, M.; Kamaras, K.; Reynolds, J. R.; Tanner, D. B.; Hebard, A. F.; Rinzler, A. G. Transparent, Conductive Carbon Nanotube Films. *Science* **2004**, *305*, 1273−1276.

(3) Grüner, G. Carbon Nanotube Films for Transparent and Plastic Electronics. *J. Mater. Chem.* **2006**, *16*, 3533−3539.

(4) Hu, L.; Hecht, D. S.; Grüner, G. Carbon Nanotube Thin Films: Fabrication, Properties, and Applications. *Chem. Rev.* **2010**, *110*, 5790−5844.

(5) Arnold, M. S.; Green, A. A.; Hulvat, J. F.; Stupp, S. I.; Hersam, M. C. Sorting Carbon Nanotubes by Electronic Structure Using Density Differentiation. *Nat. Nanotechnol.* **2006**, *1*, 60−65.

(6) Wadhwa, P.; Liu, B.; McCarthy, M. A.; Wu, Z.; Rinzler, A. G. Electronic Junction Control in a Nanotube-Semiconductor Schottky Junction Solar Cell. *Nano Lett.* **2010**, *10*, 5001−5005.

(7) Baetens, R.; Jelle, B. P.; Gustavsen, A. Properties, Requirements and Possibilities of Smart Windows for Dynamic Daylight and Solar Energy Control in Buildings: A State-of-the-Art Review. *Sol. Energy Mater. Sol. Cells* **2010**, *94*, 87−105.

(8) McCarthy, M. A.; Liu, B.; Donoghue, E. P.; Kravchenko, I.; Kim, D. Y.; So, F.; Rinzler, A. G. Low-Voltage, Low-Power, Organic Light-Emitting Transistors for Active Matrix Displays. *Science* **2011**, *332*, 570−573.

(9) Granqvist, C. G. Electrochromics for Smart Windows: Oxide-based Thin Films and Devices. *Thin Solid Films* **2014**, *564*, 1−38.

(10) Shulaker, M. M.; Hills, G.; Patil, N.; Wei, H.; Chen, H.-Y.; Wong, H.-S. P.; Mitra, S. Carbon Nanotube Computer. *Nature* **2013**, *501*, 526−530.

(11) Sangwan, V. K.; Ortiz, R. P.; Alaboson, J. M. P.; Emery, J. D.; Bedzyk, M. J.; Lauhon, L. L.; Marks, T. J.; Hersam, M. C. Fundamental Performance Limits of Carbon Nanotube Thin-Film Transistors Achieved Using Hybrid Molecular Dielectrics. *ACS Nano* **2012**, *6*, 7480−7488.

(12) Itkis, M. E.; Borondics, F.; Yu, A.; Haddon, R. C. Bolometric Infrared Photoresponse of Suspended Single-Walled Carbon Nanotube Films. *Science* **2006**, *312*, 413−416.

(13) Lu, R.; Li, Z.; Xu, G.; Wu, J. Z. Suspending Single-Wall Carbon Nanotube Thin Film Infrared Bolometers on Microchannels. *Appl. Phys. Lett.* **2009**, *94*, 163110.

(14) St-Antoine, B. C.; Ménard, D.; Martel, R. Single-Walled Carbon Nanotube Thermopile for Broadband Light Detection. *Nano Lett.* **2011**, *11*, 609−613.

(15) Yanagi, K.; Moriya, R.; Yomogida, Y.; Takenobu, T.; Naitoh, Y.; Ishida, T.; Kataura, H.; Matsuda, K.; Maniwa, Y. Electrochromic Carbon Electrodes: Controllable Visible Color Changes in Metallic Single-Wall Carbon Nanotubes. *Adv. Mater.* **2011**, *23*, 2811−2814.

(16) Wang, F.; Itkis, M. E.; Bekyarova, E.; Haddon, R. C. Charge-Compensated, Semiconducting Single-Walled Carbon Nanotube Thin Film as an Electrically Configurable Optical Medium. *Nat. Photonics* **2013**, *7*, 459−465.

(17) Moser, M. L.; Li, G.; Chen, M.; Bekyarova, E.; Itkis, M. E.; Haddon, R. C. Fast Electrochromic Device Based on Single-Walled Carbon Nanotube Thin Films. *Nano Lett.* **2016**, *19*, 5386−5393.

(18) Monroy, E.; Omnès, F.; Calle, F. Wide-Bandgap Semiconductor Ultraviolet Photodetectors. *Semicond. Sci. Technol.* **2003**, *18*, R33−R51.

(19) Liu, K.; Sakurai, M.; Aono, M. ZnO-Based Ultraviolet Photodetectors. *Sensors* **2010**, *10*, 8604−8634.

(20) Hou, Y.; Mei, Z.; Du, X. Semiconductor Ultraviolet Photodetectors Based on ZnO and $Mg_xZn_{1-x}O$. *J. Phys. D: Appl. Phys.* **2014**, *47*, 283001.

(21) Brillson, L. J.; Lu, Y. ZnO Schottky Barriers and Ohmic Contacts. *J. Appl. Phys.* **2011**, *109*, 121301.

(22) Allen, M. W.; Alkaisi, M. M.; Durbin, S. M. Metal Schottky Diodes on Zn-polar and O-polar Bulk ZnO. *Appl. Phys. Lett.* **2006**, *89*, 103520.

(23) Han, S.; Zhang, Z.; Zhang, J.; Wang, L.; Zheng, J.; Zhao, H.; Zhang, Y.; Jiang, M.; Wang, S.; Zhao, D.; Shan, C.; Li, B.; Shen, D. Photoconductive Gain in Solar-blind Ultraviolet Photodetector Based on $Mg_{0.52}Zn_{0.48}O$ Thin Film. *Appl. Phys. Lett.* **2011**, *99*, 242105.

(24) Chang, S. P.; Chang, S. J.; Chiou, Y. Z.; Lu, C. Y.; Lin, T. K.; Lin, Y. C.; Kuo, C. F.; Chang, H. M. ZnO Photoconductive Sensors Epitaxially Grown on Sapphire Substrates. *Sens. Actuators, A* **2007**, *140*, 60−64.

(25) Young, S. J.; Ji, L. W.; Chang, S. J.; Su, Y. K. ZnO Metal−Semiconductor−Metal Ultraviolet Sensors with Various Contact Electrodes. *J. Cryst. Growth* **2006**, *293*, 43−47.
(26) Lin, T. K.; Chang, S. J.; Su, Y. K.; Huang, B. R.; Fujita, M.; Horikoshi, Y. ZnO MSM Photodetectors with Ru Contact Electrodes. *J. Cryst. Growth* **2005**, *281*, 513−517.
(27) Xiu, F.; Yang, Z.; Zhao, D.; Liu, J. L.; Alim, K. A.; Balandin, A. A.; Itkis, M. E.; Haddon, R. C. ZnO Growth on Si with Low-Temperature ZnO Buffer Layers by ECR-Assisted MBE. *J. Cryst. Growth* **2006**, *286*, 61−65.
(28) Mandalapu, L. J.; Xiu, F. X.; Yang, Z.; Zhao, D. T.; Liu, J. L. P-Type Behavior From Sb-Doped ZnO Heterojunction Photodiodes. *Appl. Phys. Lett.* **2006**, *88*, 112108.
(29) Liu, J. L.; Xiu, F. X.; Mandalapu, L. J.; Yang, Z. P-type ZnO by Sb Doping for PN-junction Photodetectors. *Proc. SPIE* **2006**, *6122*, 61220H.
(30) Mandalapu, L. J.; Yang, Z.; Liu, J. L. Low-resistivity Au/Ni Ohmic Contacts to Sb-doped p-type ZnO. *App. Phys. Lett.* **2007**, *90*, 252103.
(31) Jeong, I.-S.; Kim, J. H.; Im, S. Ultraviolet-enhanced Photodiode Employing n-ZnO/p-Si Structure. *Appl. Phys. Lett.* **2003**, *83*, 2946.
(32) Zhang, T. C.; Guo, Y.; Mei, Z. X.; Gu, C. Z.; Du, X. L. Visible-blind Ultraviolet Photodetector Based on Double Heterojunction of n-ZnO/Insulator-MgO/p-Si. *Appl. Phys. Lett.* **2009**, *94*, 113508.
(33) Hou, Y. N.; Mei, Z. X.; Liang, H. L.; Ye, D. Q.; Liang, S.; Gu, C. Z.; Du, X. L. Comparative Study of n-MgZnO/p-Si Ultraviolet-B Photodetector Performance with Different Device Structures. *Appl. Phys. Lett.* **2011**, *98*, 263501.
(34) Tasi, D. S.; Kang, C. F.; Wang, H. H.; Lin, C. A.; Ke, J. J.; Chu, Y. H.; He, J. H. n-ZnO/$LaAlO_3$/p-Si Heterojunction for Visible-blind UV Detection. *Opt. Lett.* **2012**, *37*, 1112−1114.
(35) Wu, J. Z. Engineering Heterojunctions with Carbon Nanostructures: Towards High-Performance Optoelectronics. *Proc. SPIE* **2015**, *9553*, 95530Z.
(36) Bo, R.; Nasiri, N.; Chen, H.; Caputo, D.; Fu, L.; Tricoli, A. Low-Voltage High-Performance UV Photodetectors: An Interplay between Grain Boundaries and Debye Length. *ACS Appl. Mater. Interfaces* **2017**, *9*, 2606−2615.
(37) Nasiri, N.; Bo, R.; Fu, L.; Tricoli, A. Three-dimensional Nano-heterojunction Networks: a Highly Performing Structure for Fast Visible-blind UV Photodetectors. *Nanoscale* **2017**, *9*, 2059−2067.
(38) Nie, B.; Hu, J.-G.; Luo, L.-B.; Xie, C.; Zeng, L.-H.; Lv, P.; Li, F.-Z.; Jie, J.-S.; Feng, M.; Wu, C.-Y.; Yu, Y.-Q.; Yu, S.-H. Monolayer Graphene Film on ZnO Nanorod Array for High-Performance Schottky Junction Ultraviolet Photodetectors. *Small* **2013**, *9*, 2872−2879.
(39) Bai, Z.; Yan, X.; Chen, X.; Cui, Y.; Lin, P.; Shen, Y.; Zhang, Y. Ultraviolet and Visible Photoresponse Properties of a ZnO/Si Heterojunction at Zero Bias. *RSC Adv.* **2013**, *3*, 17682−17688.
(40) Liu, X.; Gu, L.; Zhang, Q.; Wu, J.; Long, Y.; Fan, Z. All-printable Band-edge Modulated ZnO Nanowire Photodetectors with Ultra-high Detectivity. *Nat. Commun.* **2014**, *5*, 4007.
(41) Guo, F.; Yang, B.; Yuan, Y.; Xiao, Z.; Dong, Q.; Bi, Y.; Huang, J. A Nanocomposite Ultraviolet Photodetector Based on Interfacial Trap-controlled Charge Injection. *Nat. Nanotechnol.* **2012**, *7*, 798−802.
(42) Ates, E. S.; Kucukyildiz, S.; Unalan, H. E. Zinc Oxide Nanowire Photodetectors with Single-Walled Carbon Nanotube Thin-Film Electrodes. *ACS Appl. Mater. Interfaces* **2012**, *4*, 5142−5146.
(43) Guo, D.-Y.; Shan, C.-X.; Qu, S.-N.; Shen, D.-Z. Highly Sensitive Ultraviolet Photodetectors Fabricated from ZnO Quantum Dots/Carbon Nanodots Hybrid Films. *Sci. Rep.* **2014**, *4*, 7469.
(44) Shao, D.; Sun, H.; Gao, J.; Xin, G.; Aguilar, M. A.; Yao, T.; Koratkar, N.; Lian, J.; Sawyer, S. Flexible, Thorn-like ZnO-multiwalled Carbon Nanotube Hybrid Paper for Efficient Ultraviolet Sensing and Photocatalyst Applications. *Nanoscale* **2014**, *6*, 13630−13636.
(45) Liu, J. S.; Shan, C. X.; Li, B. H.; Zhang, Z. Z.; Yang, C. L.; Shen, D. Z.; Fan, X. W. High Responsivity Ultraviolet Photodetector Realized Via a Carrier-Trapping Process. *Appl. Phys. Lett.* **2010**, *97*, 251102.
(46) Jin, Z.; Zhou, Q.; Chen, Y.; Mao, P.; Li, H.; Liu, H.; Wang, J.; Li, Y. Graphdiyne:ZnO Nanocomposites for High-Performance UV Photodetectors. *Adv. Mater.* **2016**, *28*, 3697−3702.
(47) Gohier, A.; Dhar, A.; Gorintin, L.; Bondavalli, P.; Bonnassieux, Y.; Cojocaru, C. S. All-printed Infrared Sensor based on Multiwalled Carbon Nanotubes. *Appl. Phys. Lett.* **2011**, *98*, 063103.
(48) Mandalapu, L. J.; Xiu, F. X.; Yang, Z.; Liu, J. L. Ultraviolet Photoconductive Detectors Based on Ga-doped ZnO Films Grown by Molecular-beam Epitaxy. *Solid-State Electron.* **2007**, *51*, 1014−1017.
(49) Kim, S.-H.; Kim, H.-K.; Seong, T.-Y. Effect of Hydrogen Peroxide Treatment on The Characteristics of Pt Schottky Contact on n-type ZnO. *Appl. Phys. Lett.* **2005**, *86*, 112101.
(50) Gu, Q. L.; Ling, C. C.; Chen, X. D.; Cheng, C. K.; Ng, A. M. C.; Beling, C. D.; Fung, S.; Djurišić, A. B.; Lu, L. W.; Brauer, G.; Ong, B. C. Hydrogen Peroxide Treatment Induced Rectifying Behavior of Au/n-ZnO Contact. *Appl. Phys. Lett.* **2007**, *90*, 122101.
(51) Gu, Q. L.; Cheung, C. K.; Ling, C. C.; Ng, A. M. C.; Djurišić, A. B.; Lu, L. W.; Chen, X. D.; Fung, S.; Beling, C. D.; Ong, H. C. Au/n-ZnO Rectifying Contact Fabricated with Hydrogen Peroxide Pretreatment. *J. Appl. Phys.* **2008**, *103*, 093706.
(52) Bonaccorso, F.; Sun, Z.; Hasan, T.; Ferrari, A. C. Graphene Photonics and Optoelectronics. *Nat. Photonics* **2010**, *4*, 611−622.
(53) Liu, H.; Sun, Q.; Xing, J.; Zheng, Z.; Zhang, Z.; Lü, Z.; Zhao, K. Fast and Enhanced Broadband Photoresponse of a ZnO Nanowire Array/Reduced Graphene Oxide Film Hybrid Photodetector from the Visible to the Near-Infrared Range. *ACS Appl. Mater. Interfaces* **2015**, *7*, 6645−6651.
(54) Gong, X.; Tong, M.; Xia, Y.; Cai, W.; Moon, J. S.; Cao, Y.; Yu, G.; Shieh, C.-L.; Nilsson, B.; Heeger, A. J. High-Detectivity Polymer Photodetectors with Spectral Response from 300 nm to 1450 nm. *Science* **2009**, *325*, 1665−1667.
(55) Henini, M.; Razeghi, M. *Handbook of Infrared Detection Technologies*; Elsevier Advanced Technology: Kidlington, Oxford, UK, 2002.
(56) Nasiri, N.; Bo, R.; Wang, F.; Fu, L.; Tricoli, A. Ultraporous Electron-Depleted ZnO Nanoparticle Networks for Highly Sensitive Portable Visible-Blind UV Photodetectors. *Adv. Mater.* **2015**, *27*, 4336−4343.
(57) Shen, Y.; Yan, X.; Si, H.; Lin, P.; Liu, Y.; Sun, Y.; Zhang, Y. Improved Photoresponse Performance of Self-Powered ZnO/Spiro-MeOTAD Heterojunction Ultraviolet Photodetector by Piezo-Phototronic Effect. *ACS Appl. Mater. Interfaces* **2016**, *8*, 6137−6143.
(58) Anderson, R. L. Experiments on Ge-GaAs Heterojunctions. *Solid-State Electron.* **1962**, *5*, 341−351.
(59) Lopez, A.; Anderson, R. L. Photocurrent Spectra of Ge-GaAs Heterojunctions. *Solid-State Electron.* **1964**, *7*, 695−700.
(60) Itkis, M. E.; Pekker, A.; Tian, X.; Bekyarova, E.; Haddon, R. C. Networks of Semiconducting SWNTs: Contribution of Midgap Electronic States to the Electrical Transport. *Acc. Chem. Res.* **2015**, *48*, 2270−2279.
(61) Behnam, A.; Johnson, J. L.; Choi, Y.; Ertosun, M. G.; Okyay, A. K.; Kapur, P.; Saraswat, K. C.; Ural, A. Experimental Characterization of Single-walled Carbon Nanotube Film-Si Schottky Contacts Using Metal-Semiconductor-Metal Structures. *Appl. Phys. Lett.* **2008**, *92*, 243116.
(62) Wang, P.-H.; Liu, B.; Shen, Y.; Zheng, Y.; McCarthy, M. A.; Holloway, P.; Rinzler, A. G. N-channel Carbon Nanotube Enabled Vertical Field Effect Transistors with Solution Deposited ZnO Nanoparticle Based Channel Layers. *Appl. Phys. Lett.* **2012**, *100*, 173514.
(63) Coppa, B. J.; Fulton, C. C.; Kiesel, S. M.; Davis, R. F.; Pandarinath, C.; Burnette, J. E.; Nemanich, R. J.; Smith, D. J. Structural, Microstructural, and Electrical properties of Gold Films and Schottky Contacts on Remote Plasma-cleaned, n-type ZnO{0001} Surfaces. *J. Appl. Phys.* **2005**, *97*, 103517.
(64) Sze, S. M. *Physics of Semiconductor Devices*; Wiley: New York, 1981.

(65) Donnelly, J. P.; Milnes, A. G. Current/Voltage Characteristics of p-n Ge-Si and Ge-GaAs Heterojunctions. *Proc. IEEE* **1966**, *113*, 1468–1476.
(66) Joshi, N. V. *Photoconductivity: Art, Science, and Technology*; Marcel Dekker, Inc.: New York, NY, 1990; Vol. *25*, p 309.
(67) Spataru, C. D.; Ismail-Beigi, S.; Benedict, L. X.; Louie, S. G. Excitonic Effects and Optical Spectra of Single-Walled Carbon Nanotubes. *Phys. Rev. Lett.* **2004**, *92*, 077402.
(68) Wang, F.; Dukovic, G.; Knoesel, E.; Brus, L. E.; Heinz, T. F. Observation of Rapid Auger Recombination in Optically Excited Semiconducting Carbon Nanotubes. *Phys. Rev. B: Condens. Matter Mater. Phys.* **2004**, *70*, 241403.
(69) Sheng, C.-X.; Vardeny, Z. V.; Dalton, A. B.; Baughman, R. H. Exciton Dynamics in Single-Walled Nanotubes: Transient Photo-induced Dichroism and Polarized Emission. *Phys. Rev. B: Condens. Matter Mater. Phys.* **2005**, *71*, 125427.
(70) Wang, F.; Dukovic, G.; Brus, L. E.; Heinz, T. The Optical Resonances in Carbon Nanotubes Arise from Excitons. *Science* **2005**, *308*, 838–841.
(71) Keem, K.; Kim, H.; Kim, G.-T.; Lee, J. S.; Min, B.; Cho, K.; Sung, M.-Y.; Kim, S. Photocurrent in ZnO Nanowires Grown from Au Electrodes. *Appl. Phys. Lett.* **2004**, *84*, 4376.
(72) Bekyarova, E.; Itkis, M. E.; Cabrera, N.; Zhao, B.; Yu, A.; Gao, J.; Haddon, R. C. Electronic Properties of Single-Walled Carbon Nanotube Networks. *J. Am. Chem. Soc.* **2005**, *127*, 5990–5995.

NOTE ADDED AFTER ASAP PUBLICATION

This paper was published on the Web on October 5, 2017, with a minor error in equation 3. The corrected version was reposted on October 9, 2017.

DOI: 10.1021/acsami.7b07765
ACS Appl. Mater. Interfaces 2017, 9, 37094–37104